Charge storage in metal-chalcogenide bilayer junctions

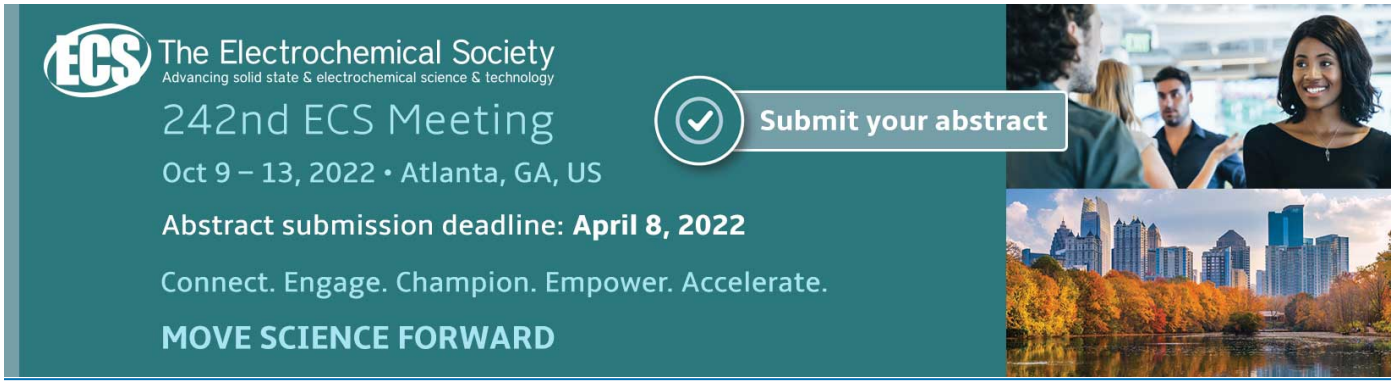

OPEN ACCESS
IOP Publishing
Journal of Physics D: Applied Physics
J. Phys. D: Appl. Phys. **54** (2021) 295105 (8pp)
https://doi.org/10.1088/1361-6463/abfbf8

Charge storage in metal-chalcogenide bilayer junctions

Y Takagaki

Paul-Drude-Institut für Festkörperelektronik, Leibniz-Institut im Forschungsverbund Berlin e.V., Hausvogteiplatz 5-7, 10117 Berlin, Germany

E-mail: takagaki@pdi-berlin.de

Received 29 January 2021, revised 7 April 2021
Accepted for publication 27 April 2021
Published 14 May 2021

Abstract

We demonstrate that electrical charges are stored in the bilayer junctions of Al and Bi–Cu–S alloys. The junctions exhibit interfacial resistance switching, which is caused by a spontaneous production of high resistivity compounds at the interface and their electrochemical dissolution under a voltage bias. The charge storage results from the redox reactions that are responsible for the resistance switching. In contrast to conventional secondary batteries, the storing capability increases as the temperature is lowered from room temperature to 77 K, where the charges are released in a time scale nearly on the order of hours. The charging and discharging are thereby indicated not to rely on ionic transport. The battery effect is reversible in polarity. Storage characteristics are modified when Cu in the ternary alloy is replaced with Ag or Ni in a similar manner to the way the properties of the interfacial resistance switching are altered.

Keywords: charge storage, chalcogenide, resistance switching

(Some figures may appear in colour only in the online journal)

1. Introduction

Battery systems that utilize metallic elements other than Li, such as Na, Mg and Al, have attracted rapidly increasing attention in recent years as post-lithium energy storage systems [1–3]. Given that Al is the most abundant metal element in the Earth's crust, a rechargeable battery based on aluminum chemistry could be a low cost energy storage system. In addition, the fact that Al is sixfold denser than Li gives rise to the approximately fourfold volumetric capacity of Al in comparison to Li. The ability to exchange three electrons as a trivalent cation Al^{3+} instead of one electron as Li^{+} also increases the energy storage capacity, which is one of the highest among all elements.

In secondary batteries, the anode and cathode are separated from each other by an aqueous or nonaqueous electrolyte [4]. Here, solid state junctions are free from the problem of instability resulting from the use of liquid electrolytes, which can be flammable [5]. In addition, a solid-state lithium battery was shown to operate in a wide temperature range down to −30 °C [6]. It is emphasized that the optimum temperature range for lithium-ion batteries is −20 °C ∼ 60 °C, where the low-temperature limit is imposed by the reduction of ionic conductivity in the electrolytes [7, 8]. Aluminum-ion batteries have been demonstrated using various metal-sulfides cathodes including Mo_6S_8, SnS_2, FeS_2, Ni_xS, CuS and Co_9S_8 [1–3, 9]. Aluminum chlorides, usually $AlCl_4^-$ or $Al_2Cl_7^-$ anions, mediate the flow of charge carriers in the electrolytes. In exploring the potential of numerous material combinations for improving the battery performance, not only experimental efforts but also the recent progresses in the computational approach of the nanobattery, where atomistic model systems are analyzed by molecular dynamics simulations [10, 11] are notable.

The junctions of metal-chalcogenides in the form of (Bi,Sb)–(Cu,Ag,Ni)–(S,Se,Te) with a metal such as Al and Ag develop a resistance switching phenomenon [12–14]. High resistivity compounds are produced at the interface by a room temperature (RT) spontaneous reaction [15]. The electrical

conduction through the junctions is consequently blocked. Chalcogens belong to the oxygen family of the periodic table. The spontaneous chemical reaction is the oxidation process of the metal. Under the application of a voltage bias to the junction, the passivation layer is decomposed by the reduction process. The electrochemical dissolution of the blocking compounds results in an abrupt switch in the junction resistance by orders of magnitude. The combination of the metal and the chalcogenide alloy determines the bias polarity for dissolving the barrier, presumably in accordance with the electronegativity of the involved elements. The resistance switching takes place at opposite bias polarities for Bi–Ag–S alloys between the cases using Al and Ag contacts [14]. The redox reactions at the interface are hence evidenced to drive this interfacial resistance switching.

The importance of such redox reactions has been established for the conventional resistive switch devices that operate based on the creation and dissolution of a metallic filament [16]. The filament connects or disconnects the electrodes through an electrolyte, giving rise to resistance switching. The oxidation, reduction and migration of metal cations in the solid electrolytes play the key roles in the transformation of the filament [17]. The switching characteristics are consequently governed by the Gibbs free energy for the formation of cations [18]. The functionalities of the resistive switch devices are attractive not only for memories [19] but also for artificial neural computing [20, 21] based on memristors [22, 23] and memristive devices [24].

It is shown in this work that the electrochemistry involved in the phenomenon of interfacial resistance switching gives rise to the storage of electrical charges in the Al-chalcogenide junctions. The application of voltages to the bilayer junctions accumulate charges of reversible polarity. The charges are released in a time scale of the order of minutes. The charging phenomenon is enhanced as the temperature is lowered from RT to 77 K. The charge storage might be utilized for realizing a solid-state rechargeable system, providing a different route for Al-based batteries, in particular, as a system that operates at ultra-low temperatures.

2. Film synthesis

Thin films of chalcogenide alloys were synthesized using the material substitution method in hot wall deposition of Bi_2S_3 layers [25–27]. When certain metals are exposed to Bi_2S_3 vapor, they replace the Bi in Bi_2S_3, forming metal sulfides. We employ here Bi–Cu–S, Bi–Ag–S and Bi–Ni–S alloys. The chalcogenide films were produced on Si substrates. The Si substrates covered with a pre-deposited layer of Cu, Ag or Ni were exposed to Bi_2S_3 vapor in vacuum for 4 h at temperature T_s. The thickness of the Cu, Ag and Ni layers was 40, 80 and 60 nm, respectively. The ternary alloys were obtained by this procedure as the substitution of Bi was partial. Chalcogenides can exist with various compositions and polymorphs. The synthesized materials, therefore, changed widely with T_s. The compositions of the chalcogenide alloys were examined using x-ray crystallography. The details of the synthesis and the structural and electrical properties of the alloy films can be found in [13, 14]. We point out that the charge storage phenomenon to be demonstrated below is expected not to be affected significantly by the specific composition of the chalcogenide alloys as the interfacial resistance switching was observed for samples prepared in a wide range of T_s [14].

3. Results and discussion

The variation of the sheet resistivity ρ_s of the alloy films with T_s was investigated in [14]. The change of ρ_s of the Bi–Cu–S films with T_s was over five orders of magnitude, ranging from metallic to significantly resistive conduction. The conduction in the Bi–Ag–S films was as resistive as in the high resistivity Bi–Cu–S films while ρ_s changed with T_s in less than one order of magnitude. For the Bi–Ni–S films, ρ_s was similarly high, in general, regardless of T_s. Exceptions, however, existed exhibiting abrupt decreases of ρ_s in several orders of magnitude for some values of T_s. The specific compositions of the Bi–Ni–S alloys realized in the films were presumably responsible for the metallic conduction.

Figure 1 shows the dependencies of ρ_s of the chalcogenide films on temperature T. The Bi–Ag–S, Bi–Ni–S and Bi–Cu–S films were produced at $T_s = 151, 299$ °C and 177 °C, respectively. These samples were chosen among the films prepared at various T_s as they were the cases of low ρ_s for each alloy. The metallic behavior of decreasing ρ_s with lowering T was observed, as a consequence, for the Bi–Ni–S and Bi–Cu–S films in figures 1(b) and (c), respectively. Due to the absence of such a low-ρ_s sample for the Bi-Ag-S films, one finds freezing of free carriers with lowering T in figure 1(a). Here, the thermal activation energy was deduced to be $E_a = 0.26$ eV. It may be noteworthy that the possibility of the large values of ρ_s for the Bi–Ag–S films being due to the formation of a barrier at the contacts was ruled out by careful examinations of the voltage–current (V–I) characteristics of the ohmic contacts used in the electrical measurements.

It is pointed out that the chalcogenide films were not homogeneous. To be specific, microcrystals were generated during the film synthesis [27]. The microcrystals were generally more conductive than the underlying layers. The distribution of the microcrystals was nevertheless sparse. The underlying layers of the chalcogenide films hence determined ρ_s predominantly rather than the microcrystals. The Bi–Ni–S film contained α-NiS as the microcrystals, which was revealed by x-ray crystallography [27]. Bulk α-NiS undergoes a first-order transition between a semiconducting antiferromagnetic phase and a metallic paramagnetic phase at a Neel temperature of about 263 K [28–30]. The absence of an anomaly in the temperature dependence originating from the phase transition despite the inclusion of α-NiS in the film supports the insignificant role of the microcrystals for ρ_s. In contrast to such a situation in figure 1, the microcrystals also play a role for the metal-chalcogenide junctions investigated below since the metal contact is attached to both the microcrystals and the underlying layer.

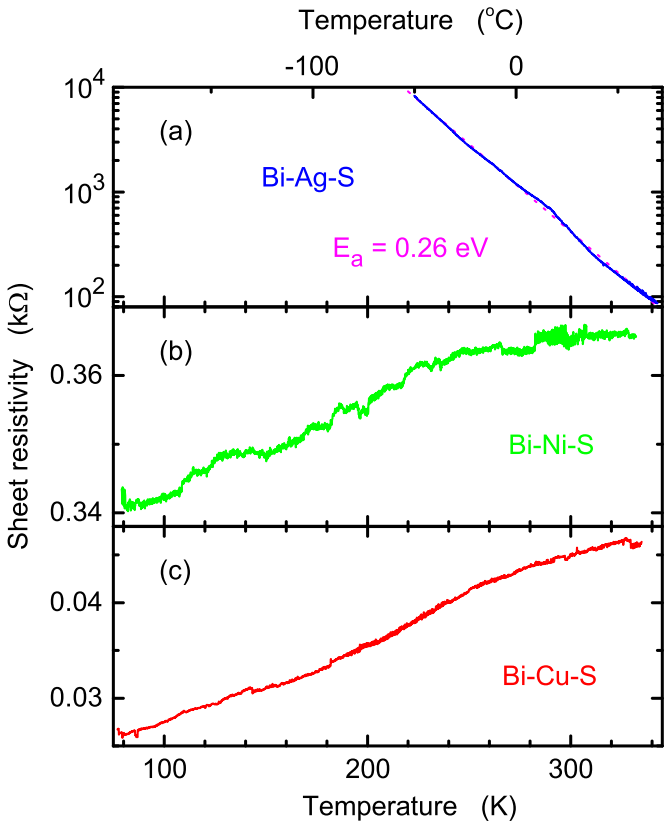

Figure 1. Temperature dependence of sheet resistivity ρ_s of chalcogenide films. The Bi–Ag–S, Bi–Ni–S and Bi–Cu–S films in (a)–(c) were synthesized at temperatures of $T_s = 151$ °C, 299 °C and 177 °C, respectively. The thermal activation energy in (a) is deduced to be $E_a = 0.26$ eV, as shown by the dotted line.

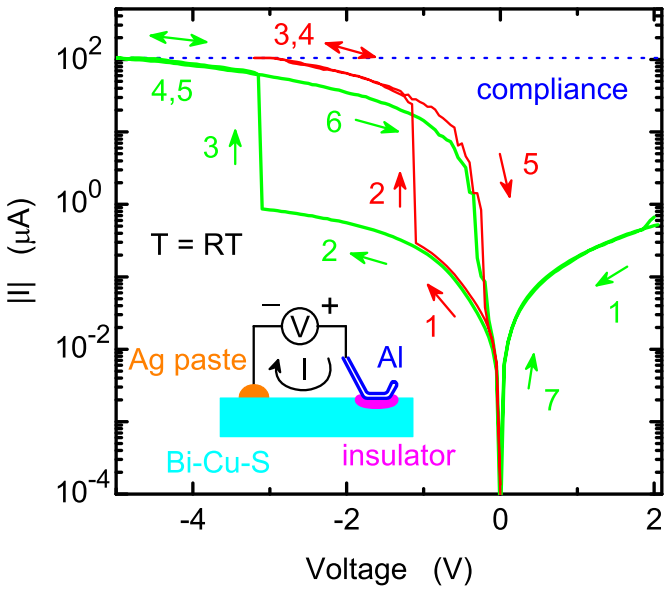

Figure 2. Interfacial resistance switching in Al/Bi–Cu–S junction at room temperature. Two resistance switching cycles are shown by the red and green curves. The numbered arrows indicate the sequence of the voltage sweeps with the sweep direction. The compliance of the source measure unit is indicated by the blue dotted line. The Al/Bi–Cu–S junction is illustrated in the inset. An Al wire was attached to the Bi–Cu–S film by means of ultrasonic bonding. An insulator layer is formed at the interface due to a spontaneous chemical reaction. The V–I characteristics were obtained by applying a voltage V to the Al lead with respect to an ohmic contact of the Bi–Cu–S film prepared using a silver paste.

Let us first demonstrate the interfacial resistance switching using an Al/Bi–Cu–S junction [25–27]. The Al contact was prepared by means of ultrasonic bonding of an Al wire, as illustrated in the inset of figure 2. The wire with a diameter of 25 μm was pressed to the Bi–Cu–S film to form the junction with an expanded width of about 100 μm of the Al contact over a length of several hundred μm [25]. It is emphasized that the microcrystals in the chalcogenide film were mashed and mixed with the underlying layer in the bonding process as chalcogenides are softer than Al. The situation may be described as attaching an Al wire to the Si substrate using the chalcogenide film as an adhesion layer.

In figure 2, V–I characteristics of the Al/Bi–Cu–S junction are shown. The bias was applied to the Al contact relative to an ohmic contact of the Bi–Cu–S film prepared using a silver paste. Two examples of the resistance switching behavior are shown by the red and green curves. The numbered arrows indicate the sequences the bias was varied. As V changed from 0 to -3.2 V in the red curve, the current was small initially due to the presence of the spontaneously created interface barrier between the Al lead and the Bi–Cu–S film, see the inset of figure 2. The dissolution of the barrier gave rise to an abrupt increase of $|I|$ at $V = -1.1$ V, as indicated by the red arrow 2. It is apparent from the abrupt increase of the current in two orders of magnitude that the small current at the low voltages is not due to the formation of a Schottky barrier at the interface. The barrier remained to be absent until its spontaneous regeneration when V was changed to be around zero. The barrier in the interfacial resistance switching can be strengthened by applying an opposite bias prior to the induction of the barrier dissolution [25–27]. As one finds in the green curve, the switch voltage shifted to -3.1 V when the bias sweep started from 2 V. It is demonstrated below that this alteration of the switch voltage is, in fact, accompanied with storing electrical charges in the Al/Bi–Cu–S junction. It is noted that a similar battery effect has been reported for memristive systems, which can be a factor that influences the functionality as an artificial neuromorphic element [31–33]. The Nernst, diffusion and Gibbs-Thomson potentials of non-equilibrium states were pointed out as the origin of the electromotive force [31].

In figure 3(a), the current flow in the Al/Bi–Cu–S junction was monitored when the bias applied to the junction was varied in step-wise manners as shown by the green curve. When the bias was turned off to be zero abruptly from finite values, the current did not vanish immediately. In the case where a bias of 20 V was applied for 1 min, the current fell to be below the detection limit ($\sim$0.4 nA) nearly half an hour after the turning off of the bias. That is, the current decreased by two orders of magnitude in 30 min. This charge release corresponds to storing electrons in the interface area of the device with a density of $\sim 10^{21}$ m^{-2}. The amplitude and the decay characteristics of the zero-bias current did not appear to depend crucially on the

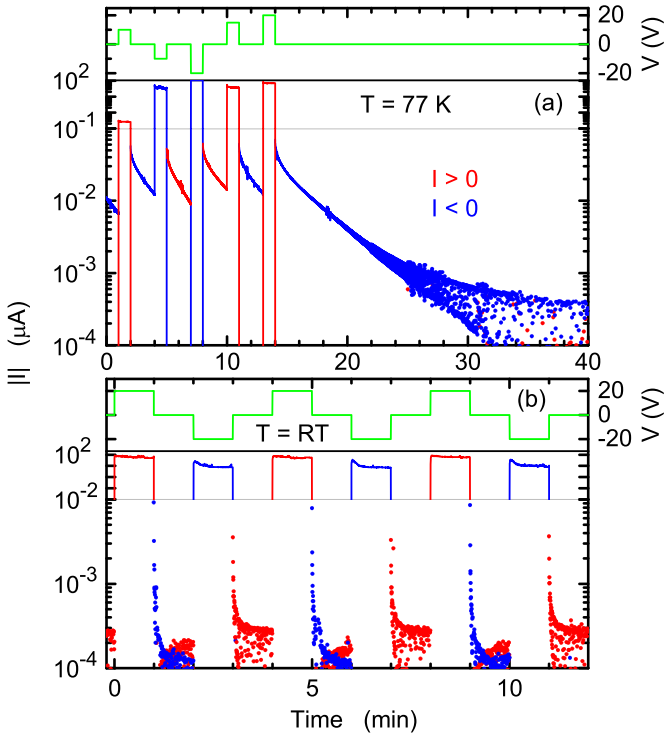

Figure 3. Charge release from Al/Bi–Cu–S junction. Time evolutions of the current I are shown when the voltage bias V applied to the junction was varied in step-wise manners as shown by the green curve. The temperature T was (a) 77 K and (b) room temperature. Positive and negative values of I are shown in red and blue, respectively. The voltage was applied to the Al contact with respect to the Bi–Cu–S film. The scale of $|I|$ is changed at (a) 10^{-1} μA and (b) 10^{-2} μA.

polarity and the strength of the bias that charged the junction for $|V| \geq 10$ V. As an energy storage system, the device hence works as a battery of invertible polarity.

Since the absolute value $|I|$ of the current is plotted in figure 3, the positive and negative currents are distinguished by the red and blue curves, respectively. One notices that the polarity of the current while $V = 0$ is opposite to that in the preceding charging procedure. This polarity reversal evidences that the zero-bias current did not originate from, for instance, the charging of deep trap levels. Such a space charge sustains the potential profile that was present under the strong bias, and so the polarity of the transient current remains the same. We will return to this point later. The curves exhibiting the decay of the current under $V = 0$ were nearly identical regardless of whether the charging biases with the same polarity or alternating polarities were applied in the sequence. The junction was hence manifested to be almost fully charged by an application of large $|V|$ ($\geq$10 V) for 1 min independent of the existing charge state.

The measurement in figure 3(a) was carried out, in fact, at $T = 77$ K since the charging effect was enhanced with lowering T. The effect was recognizable even at RT, as shown in figure 3(b). Here, the charge release from the junction was monitored following alternate applications of $\pm$20 V for 1 min. The current flowing out of the junction under zero bias was a few orders of magnitude smaller at RT than at $T =$ 77 K. The current thus vanished in less than 1 min. Nevertheless, the characteristic reversal in the polarity of the current between the charging and discharging situations is apparent. Note that the asymmetry in the background current between the cases of the charging performed with $V > 0$ and $V < 0$ is due to the offset of the source measure unit. It is noticed that the current in the charging procedure also exhibits a transient behavior with a time scale similar to that in the discharging. Conventional batteries such as lithium- and aluminum-ion batteries cannot operate at temperatures such as 77 K due to the decrease of ionic conductivity [6–8]. The present device operates as a charge storage system apparently without relying on the ionic charge transport. The generation of electromotive forces has been investigated for the memristive system that operates based on the filamentation conduction [31, 34], where the battery behaviour was found to be affected by the moisture incorporated in the electrolytes [31, 35–37]. The role of the moisture is anticipated to be insignificant at $T = 77$ K.

Concerning the measurements at $T =$ RT shown in figures 2 and 3(b), the following needs to be explicitly stated. While an interface barrier that is sufficient to block the current in the junction is formed quickly in the absence of a voltage bias, the barrier builds up further with time as the interface reaction continues to generate resistive compounds. The resistance switching voltage becomes, as a consequence, exceptionally large in the switching cycle after a long idle time of, for instance, days [25–27]. The two switching cycles presented in figure 2 were obtained after an activation of the device, where the slowly accumulated thick interface barrier was dissolved by applying a strong negative voltage. Once the junction interface has been made transparent by this clearing procedure, the resistance switching takes place at small voltages, as determined by the rapid component of the interface reaction. In figure 3(b), the junction was not activated yet in this accord, making it possible to apply the strong bias voltages of $\pm$20 V to the junction without causing the current to exceed the compliance of the source measure unit. In other words, the interfacial resistance switching did not take place in figure 3(b) since the bias voltage required to cause the initial resistance switching exceeded $-$20 V.

The consequences of the temperature dependence of the redox reactions on the interfacial resistance switching are shown in figure 4. While the V–I characteristics of the Al/Bi–Cu–S junction were measured at $T = 77$ K, the absolute value of the DC resistance $|V/I|$ is plotted in figure 4 for a better presentation of the behavior. Figure 4(a) corresponds to the situation of the interfacial resistance switching in figure 2. The electrochemical dissolution of the interface barrier was, in principle, not affected by the lowering of temperature, and so the resistance switching was induced in the first measurement cycle shown in red at $-$18 V. It is likely that such a strong bias was necessary to induce the switching because this was the activation procedure of the device, as we mentioned above, rather than a temperature effect. The junction resistance around $V = 0$ became as high as the value before the initial dissolution of the interface barrier. However, no abrupt resistance switching appeared in the additional bias sweeps. This implies

that the interface barrier was not restored to block the conduction when the bias was reduced to zero due to the freezing of the ionic transport at low temperatures. The roughly symmetric shape of the curves under reversal of V supports the absence of the interface barrier. The blocking of the conduction around $V = 0$ is suggested to be caused by the charges that were accumulated in the junction. While the interfacial resistance switching does require the ionic transport associated with redox reactions for its emergence, the charges are stored and released regardless of the ionic transport. Although the mechanism of the charge storage is unknown at present, the existence of an unconventional route for realizing a charge storage system is manifested.

The rest of the panels (b)–(e) of figure 4 show the characteristics when the interfacial resistance switching was not activated, i.e. they correspond to the situation in figure 3. The behavior we discuss below was, nonetheless, the same for both figures 4(a) and (b)–(e). The variations of $|V/I|$ in a series of voltage sweeps with alternating sweep directions are shown in separate panels as figures 4(b)–(e) in the descending order. The numbered arrows again indicate the sequence and the direction of the voltage sweeps. In figure 4(b), for instance, V was changed from 0 to −21 V as shown by the red curve and then from −21 V to 21 V as shown by the green curve. One finds in the green curve that $I = 0$ was realized before V reached 0 [31, 38], resulting in the divergence of the resistance. Note that V/I is negative between the divergence and $V = 0$. This also means that $|V/I|$ diminishes around $V = 0$ due to the sign change. The subsequent bias sweeps in figure 4(c) reveal that the application of both positive and negative biases caused $I = 0$ to emerge ahead of $V = 0$. Considering also the increase of the resistance around $V = 0$ in figure 4(a), it is speculated that a dipole layer, which was reversible in polarity, was formed in the charging process, causing the shift of the voltage for $I = 0$. If the transient behavior arising from extremely slow charge release of deep levels is responsible for the shift, $I = 0$ should appear after the voltage sweep crossed $V = 0$.

The negligible role of the thickness of the interface barrier in the comparison between figures 4(a) and (b)–(e) may suggest that the charges are stored not at the Al/Bi–Cu–S interface but at the interface that the highly resistive Al–Bi–Cu–S compounds form with the Bi–Cu–S alloy or with Al. It is emphasized that the absence of the interfacial resistance switching in figure 4(a) does not mean the complete absence of the highly resistive compounds in the junction. There are evidences that indicate that the resistance switching takes place by creating pinholes in the barrier layer, thereby causing a short-circuit of the junction, rather than dissolving the entire barrier layer. In [12], the interfacial resistance switching was observed to occur in a device where the contact was prepared by depositing a millimeter-size Al pad instead of bonding the Al wire. The resistance switching did not occur initially due to the short-circuiting of the junction in defective areas of such a large Al contact [35]. When the switching eventually took place about a year after the contact preparation thanks to the gradual lateral expansion of the interface barrier over the entire interface, the current was on the order of magnitude that is typically obtained for the devices prepared using the Al wires. This indicates that

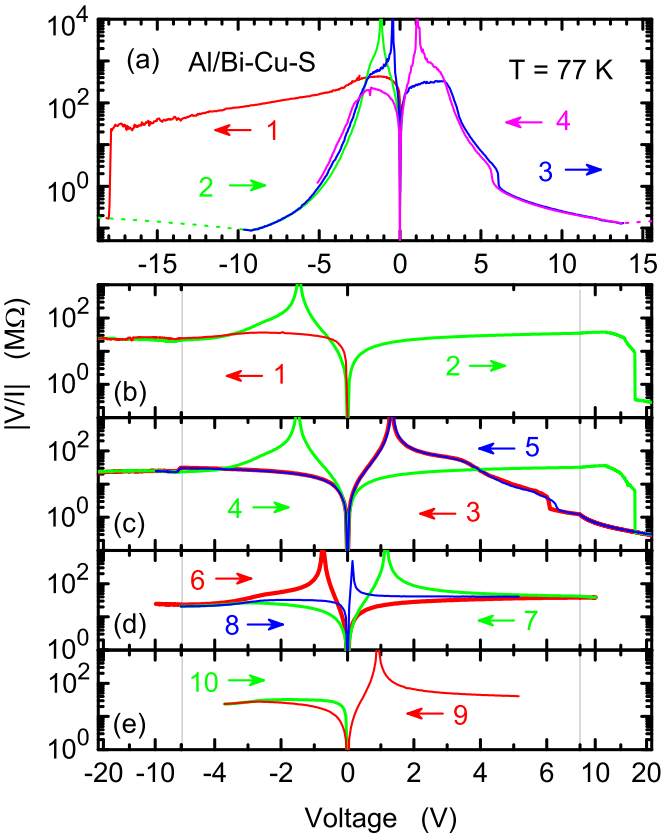

Figure 4. Variation of resistance V/I with voltage V for Al/Bi–Cu–S junction at temperature $T = 77$ K. The numbered arrows show the sequence and direction of voltage sweeps. The resistance is plotted using the absolute value as it is negative between its divergence and $V = 0$. An interfacial resistance switching was induced at −18 V in (a) in the initial sweep shown in red. The resistance could not be measured for the parts shown as dotted curves since the current exceeded the compliance of the source measure unit. Interfacial resistance switching in negative voltages was not induced in the situation shown in (b)–(e). The voltage was applied to the Al contact with respect to the Bi–Cu–S film. The bias was swept at a rate of 0.5 V s^{-1}.

the switching events are caused by just a small number of such pinholes regardless of the size of the Al contact.

The resistance around $V = 0$ plausibly increased in the situation in figure 4(a) as the dipole field suppressed the transit of electrons through the pinholes. As an example of the formation of a dipole in a similar system, we point out the interface of high-k dielectrics and SiO_2 [39, 40]. Here, the transient current exhibits an enhancement with increasing the charging bias. The temperature dependence in this case is given by the thermal activation in orienting the dipole to the direction of the electric field.

In figures 4(d) and (e), the voltage at which $I = 0$ occurred moved towards zero when the bias to charge the junction was weakened. The reproducibility of the null-current voltage for identical charging conditions was, on the other hand, obvious in figures 4(b) and (c). The blue curve in figure 4(d) shows that the polarity of the charges in the junction was not inverted by the application of −5 V. The following application of 5 V, in contrast, enhanced the charging significantly, as shown by

the red curve in figure 4(e). Together with the difference in the null-current voltage of −1.5 and 1.3 V for applications of, respectively, −21 V and 21 V in figure 4(c), an asymmetry between the positively and negatively biased situations is suggested to be present. The absence of the charge polarity reversal in the weak biasing was affirmed by the green curve in figure 4(e).

The charge storage was observed also when Bi–Ag–S and Bi–Ni–S alloys were employed instead of the Bi–Cu–S alloy. For the Bi–Ag–S films, the measurements were not possible at low temperatures as the conduction had to be activated thermally. The behavior in an Al/Bi–Ag–S junction at $T =$ RT is shown by the red curve in figure 5(a). Here, the Bi–Ag–S film was prepared at $T_s = 325$ °C. The magnitude of the discharge current was comparable to that for the Bi–Cu–S film. Note that the ohmic contact to the Bi–Ag–S film was fabricated by depositing a Au contact pad since the Ag paste reacts with Bi–Ag–S alloys, generating an electrochemically decomposable interface barrier [14]. For this reason, we have examined the battery effect also for a Ag/Bi–Ag–S junction, as shown by the blue curve in figure 5(a). Charges are seen to be gradually released, similar to the Al/Bi–Cu–S and Al/Bi–Ag–S junctions, following a negative biasing of the contact made of the Ag paste with respect to the Au contact. The decay of the current was much faster for the positive charging. Note that the absence of the charge storage behavior was confirmed when the measurements were carried out between two Au contacts.

The properties of the discharge current were asymmetric between positive and negative charging for the cases of the Bi–Ag–S film. The charging polarity for achieving stronger charge accumulation was reversed between the cases of using the Al and Ag contacts. This reminds us of the opposite bias polarities in operating the interfacial resistance switching between these cases [14]. The discharge current was larger for the bias that strengthens the interface barrier in the interfacial resistance switching. This is consistent with the interpretation that the bias-induced shift in the resistance switching voltage arises from the charge storage.

For the Al/Bi–Ag–S junction, the charging was independent of the existing charge state, similar to the Al/Bi–Cu–S junction. In contrast, the charge storage was enhanced for the Ag/Bi–Ag–S junction in the consecutive applications of −20 V. The difference appears to be related to the slow decay of the discharge current for the Ag contact. Moreover, the charging under the negative bias was significantly reduced after the application of a bias of 20 V. The interface barrier in Ag/Bi–Ag–S junctions is dissolved by a positive biasing. The amount of the residual barrier compounds was plausibly reduced here, and so the charge storage capacity was lowered. Note that the original storing capacity was regained with the recovery of the interface barrier when the device was left idle.

The generation of resistive compounds with Al is much slower for Bi–Ni–S alloys than for Bi–Cu–S alloys [14]. The discharge current was undetectable for the film used in figure 1(b) as the conduction in the junction with Al was metallic due to negligible interface barrier. The junction resistance, nonetheless, increased by orders of magnitude for

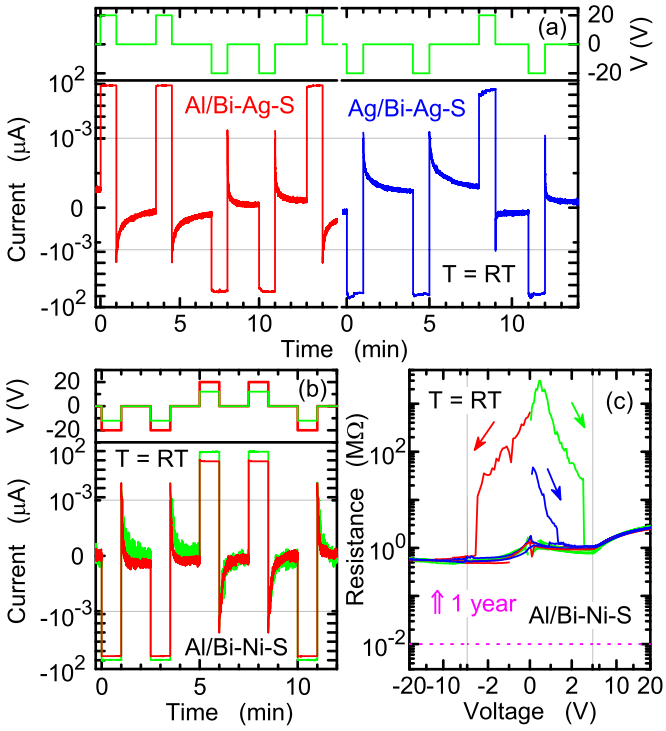

Figure 5. Charging and discharging current transients for (a) Bi–Ag–S and (b) Bi–Ni–S films. The red and blue curves in (a) show the current when, respectively, Al and Ag contacts on the Bi–Ag–S film were biased with respect to a Au contact at room temperature. The voltage applied to the junctions is shown by the green curves. The Bi–Ag–S film was grown at $T_s = 325$ °C. The vertical scale is changed at $I = -6 \times 10^{-4}$ and 10^{-3} μA. The Bi–Ni–S films corresponding to the red and green curves in (b) were grown at $T_s = 327$ °C and 379 °C, respectively. The current in the Al/Bi–Ni–S junctions is plotted with changing the scale at $\pm 5 \times 10^{-4}$ μA. The offset of the source measure unit has been corrected in (a) and (b). The bias dependence of the resistance of the Al/Bi–Ni–S junction is shown in (c) for $T_s = 327$ °C. The device was left idle for ≈100 ds for the red and green curves and 1 day for the blue curve prior to the measurements. The arrows indicate the initial part of the sweeps that started from $V = 0$. The dotted line indicates the resistance immediately after the preparation of the Al contact, which was a year before the measurements. The scale of the voltage is changed at ±3 V. The bias sweep rate was 1 V s^{-1} for the red and green curves and 0.5 V s^{-1} for the blue curve.

some Bi–Ni–S films prepared at different T_s 1 year after the Al contact preparation. These junctions exhibited discharge currents at RT, which were almost identical to each other as shown in figure 5(b). Here, the red and green curves correspond to films with $T_s = 327$ °C and 379 °C, respectively. The current transients in the discharging were nearly the same between positive and negative biasing. The Bi–Ni–S films thus resembled the Bi–Cu–S films in this respect.

The bias dependence of the resistance of the Al/Bi–Ni–S junction investigated above is shown in figure 5(c) for the film with $T_s = 327$ °C. The red and green curves manifest that the initial resistance was extremely large. The barrier was eliminated by the application of a voltage of ±2.6 V regardless of the polarity. It is seen that the slow interface reaction was unable to regenerate the barrier for the bias sweep rate in figure 5(c). The

thick barriers evident in the red and green curves were established cumulatively during a period of about 100 d. The barrier that was built by leaving the junction idle for 1 d is found in the blue curve. The measurements in figure 5(b) were performed after the dissolution of the interface barrier. The junction resistance was significantly large even after the dissolution of the interface barrier compared to that just after the preparation of the Al contacts, which is indicated by the dotted line. This is, in fact, another evidence that suggests that the barrier layer was not entirely decomposed by the biasing, as discussed above. There seems to exist no correlation between the time scale for creating the barrier layer and the decay time of the discharge current.

4. Conclusions

In conclusion, gradual releases of electrical charges in a time scale on the order of minutes have been demonstrated using the bilayer junctions of Al and Bi–M–S alloys with M = Cu, Ni and Ag and Ag/Bi–Ag–S junctions. The polarity of the current in the discharging process is opposite to that in the preceding charging procedure where a large voltage is applied to the junction. The current flow at zero bias is thus indicated to originate from a storage of charges. The charge accumulation is related to the interfacial resistance switching phenomenon that the junctions exhibit through the redox reactions at the junction interface. The storing capacity increases by orders of magnitude with lowering temperature, which is in contrast to the disappearance of the interfacial resistance switching at low temperatures. The charges are thus manifested to be held without relying on the ionic transport in the electrolyte. Although the charge storage presented in this work is not competitive at all with existing batteries, the storage excels at ultra-low temperatures, where conventional batteries have no chance to accomplish the required task.

Data availability statement

The data that support the findings of this study are available upon reasonable request from the authors.

ORCID iD

Y Takagaki https://orcid.org/0000-0002-6691-1005

References

[1] Hu Y, Sun D, Luo B and Wang L 2019 Recent progress and future trends of aluminum batteries *Energy Technol.* **7** 86–106
[2] Leisegang T *et al* 2019 The aluminum-ion battery: a sustainable and seminal concept? *Frontiers Chem.* **7** 268
[3] Yuan D, Zhao J, Manalastas J W, Kumar S and Srinivasan M 2020 Emerging rechargeable aqueous aluminum ion battery: status, challenges and outlooks *Nano Mater. Sci.* **2** 248–63
[4] Borah R, Hughson F R, Johnston J and Nann T 2020 On battery materials and methods *Mater. Today Adv.* **6** 100046
[5] Hu Y-S 2016 Getting solid *Nat. Energy* **1** 16042
[6] Kato Y, Hori S, Saito T, Suzuki K, Hirayama M, Mitsui A, Yonemura M, Iba H and Kanno R 2016 High-power all-solid-state batteries using sulfide superionic conductors *Nat. Energy* **1** 16030
[7] Ma S, Jiang M, Tao P, Song C, Wu J, Wang J, Deng T and Shang W 2018 Temperature effect and thermal impact in lithium-ion batteries: a review *Prog. Nat. Sci.: Mater. Intern.* **28** 653–66
[8] Mukai K, Inoue T, Kato Y and Shirai S 2017 Superior low-temperature power and cycle performances of Na-ion battery over Li-ion battery *ACS Omega* **2** 864–72
[9] Ali Zafar Z, Imtiaz S, Razaq R, Ji S, Huang T, Zhang Z, Huang Y and Anderson J A 2017 Cathode materials for rechargeable aluminum batteries: current status and progress *J. Mater. Chem.* **5** 5646–60
[10] Ponce V, Galvez-Aranda D E and Seminario J M 2017 Analysis of a Li-ion nanobattery with graphite anode using molecular dynamics simulations *J. Phys. Chem.* C **121** 12959–71
[11] Ponce V, Galvez-Aranda D E and Seminario J M 2021 Analysis of an all-solid state nanobattery using molecular dynamics simulations under an external electric field *Phys. Chem. Chem. Phys.* **23** 597–606
[12] Takagaki Y, Ramsteiner M, Jahn U, Jenichen B and Trampert A 2019 Memristive resistive switch based on spontaneous barrier creation in metal-chalcogenide junctions *J. Phys. D: Appl. Phys.* **52** 385101
[13] Takagaki Y, Jenichen B, Ramsteiner M and Trampert A 2020 Interfacial resistance switching characteristics in metal-chalcogenide junctions using Bi–Cu–Se, Bi–Ag–Se and Sb–Cu–Te alloys *J. Alloys Compd.* **824** 153880
[14] Takagaki Y, Jenichen B, Ramsteiner M and Herfort J 2021 Dependence of interfacial resistance switching on transition metal constituent M = Cu, Ag and Ni for chalcogenides Bi-M-S *J. Alloys Compd.* **858** 157709
[15] Cho D-Y, Luebben M, Wiefels S, Lee K-S and Valov I 2017 Interfacial metal–oxide interactions in resistive switching memories *ACS Appl. Mater. Interfaces* **9** 19287–95
[16] Ielmini D 2016 Resistive switching memories based on metal oxides: mechanisms, reliability and scaling *Semicond. Sci. Technol.* **31** 063002
[17] Valov I, Sapezanskaia I, Nayak A, Tsuruoka T, Bredow T, Hasegawa T, Staikov G, Aono M and Waser R 2012 Atomically controlled electrochemical nucleation at superionic solid electrolyte surfaces *Nat. Mater.* **11** 530–5
[18] Lübben M and Valov I 2019 Active electrode redox reactions and device behavior in ECM type resistive switching memories *Adv. Electron. Mater.* **5** 1800933
[19] Waser R and Aono M 2007 Nanoionics-based resistive switching memories *Nat. Mater.* **6** 833–40
[20] Ielmini D and Wong H-S P 2018 In-memory computing with resistive switching devices *Nat. Electron.* **1** 333–43
[21] Zidan M A, Strachan J P and Lu W D 2018 The future of electronics based on memristive systems *Nat. Electron.* **1** 22–9
[22] Chua L O 1971 Memristor–the missing circuit element *IEEE Trans. Circuit Theory* **CT-18** 507–19
[23] Chua L O 2011 Resistance switching memories are memristors *Appl. Phys.* A **102** 765–83
[24] Chua L O and Kang S M 1976 Memristive devices and systems *Proc. IEEE* **64** 209–23
[25] Takagaki Y, Ramsteiner M, Jahn U and Jenichen B 2019 Constituent substitution in hot wall deposition of Bi_2S_3 films by reaction with substrates *J. Solid State Chem.* **270** 219–25
[26] Takagaki Y, Jahn U, Ramsteiner M and Friedland K-J 2011 Substitution of bismuth in hot wall epitaxy of Bi_2S_3 on transition metals *Semicond. Sci. Technol.* **26** 085031

[27] Takagaki Y, Jahn U and Ramsteiner M 2012 Incorporation of transition metals in the hot-wall-epitaxy growth of Bi_2Te_3 and Sb_2Te_3 *Semicond. Sci. Technol.* **27** 085006
[28] Tsubokawa I 1958 On the magnetic properties of nickel sulfide *J. Phys. Soc. Japan* **13** 1432–8
[29] Sparks J T and Komoto T 1967 Metal-to-semiconductor transition at the magnetic ordering temperature of NiS *Phys. Lett.* A **25** 398–9
[30] Sparks J T and Komoto T 1968 Metal-to-semiconductor transition in hexagonal NiS *Rev. Mod. Phys.* **40** 752–4
[31] Valov I, Linn E, Tappertzhofen S, Schmelzer S, van den Hurk J, Lentz F and Waser R 2013 Nanobatteries in redox-based resistive switches require extension of memristor theory *Nat. Comm.* **4** 1771
[32] Tappertzhofen S, Linn E, Böttger U, Waser R and Valov I 2014 Nanobattery effect in RRAMs−Implications on device stability and endurance *IEEE Electro. Device Lett.* **35** 208–10
[33] Mai V H *et al* 2015 Memristive and neuromorphic behavior in a Li_xCoO_2 nanobattery *Sci. Rep.* **5** 7761
[34] Hu Q, Li R, Zhang X, Gao Q, Wang M, Shi H, Xiao Z, Chu P K and Huang A 2019 Lithium ion trapping mechanism of SiO_2 in $LiCoO_2$ based memristors *Sci. Rep.* **9** 5081
[35] Lübben M, Cüppers F, Mohr J, von Witzleben M, Breuer U, Waser R, Neumann C and Valov I 2020 Design of defect-chemical properties and device performance in memristive systems *Sci. Adv.* **6** eaaz9079
[36] Valov I and Tsuruoka T 2018 Effects of moisture and redox reactions in VCM and ECM resistive switching memories *J. Phys. D: Appl. Phys.* **51** 413001
[37] Tappertzhofen S, Waser R and Valov I 2014 Impact of the counter electrode material on redox processes in resistive switching memories *ChemElectroChem* **1** 1287–92
[38] Sun B, Xiao M, Zhou G, Ren Z, Zhou Y N and Wu Y A 2020 Non-zero-crossing current-voltage hysteresis behavior in memristive system *Mater. Today Adv.* **6** 100056
[39] Papaioannou G and Plana R 2010 *Advanced Microwave and Millimeter Wave Technologies: Semiconductor Devices, Circuits and Systems* ed M Mukherjee (Rijeka: InTech) p 275
[40] Engström O, Raeissi B, Piscator J, Mitrovic I Z, Hall S, Gottlob H D B, Schmidt M, Hurley P K and Cherkaoui K 2010 Charging phenomena at the interface between high-*k* dielectrics and SiO_x interlayers *J. Telecomm. Inf. Technol.* 10–19